Effective diffusion coefficients in random packings of polydisperse hard spheres from two-point and three-point correlation functions

D. Hlushkou, H. Liasneuski, U. Tallarek, and S. Torquato

Citation: Journal of Applied Physics **118**, 124901 (2015); doi: 10.1063/1.4931153
View online: http://dx.doi.org/10.1063/1.4931153
View Table of Contents: http://scitation.aip.org/content/aip/journal/jap/118/12?ver=pdfcov
Published by the AIP Publishing

JOURNAL OF APPLIED PHYSICS **118**, 124901 (2015)

Effective diffusion coefficients in random packings of polydisperse hard spheres from two-point and three-point correlation functions

D. Hlushkou,[1] H. Liasneuski,[1,2] U. Tallarek,[1,a)] and S. Torquato[3,a)]
[1]*Department of Chemistry, Philipps-Universität Marburg, Hans-Meerwein-Strasse 4, 35032 Marburg, Germany*
[2]*Department of System Analysis and Computer Simulation, Belarusian State University, Kurchatov Street 5, 220050 Minsk, Belarus*
[3]*Department of Chemistry, Department of Physics, Program in Applied and Computational Mathematics, Princeton Institute for the Science and Technology of Materials, Princeton University, Princeton, New Jersey 08544, USA*

(Received 25 May 2015; accepted 6 September 2015; published online 23 September 2015)

We evaluate the effective diffusion coefficient D_{eff} in random packings of polydisperse hard spheres with an analytical formula involving the three-point microstructural parameter ζ_2. Bulk packings with solid volume fraction between $\phi = 0.54$ and $\phi = 0.634$ were computer-generated using experimentally determined particle size distributions characterized by different mean particle diameter and associated standard deviation. The parameter ζ_2 was calculated from two- and three-point correlation functions S_2 and S_3, respectively, via an approach based on sampling templates. Results of the asymptotic analysis for S_2 and S_3 compare favorably with theoretical predictions. Effective diffusivities calculated by the approximate analytical formula are close to those obtained from simulations using a random-walk particle-tracking technique. The values of D_{eff} are affected by the packings' solid volume fraction, the spatial positions of the spheres, and to a far lesser extent by the particles' polydispersity. The proposed numerical approach can be applied to evaluate effective diffusive transport properties of general two-phase materials just from the geometrical information embodied in ϕ and ζ_2. © *2015 AIP Publishing LLC*.
[http://dx.doi.org/10.1063/1.4931153]

I. INTRODUCTION

Direct determination of the effective transport properties of a disordered multiphase medium from its microstructure is an outstanding scientific problem.[1–6] A wide class of naturally occurring and synthetic two-phase media are composed of discrete particles with different size. Typical examples of these media include soil, packed columns for catalytic reactions or chromatographic separations, battery electrodes, etc. In view of the random, complex geometry of real composite materials, an exact analytical prediction of the effective properties cannot be made even for the simplest class of transport processes, such as diffusion or electrical and thermal conduction, governed by a steady-state diffusion equation because, in principle, an infinite amount of microstructural information in the form of n-point correlation functions is required.[1] A conventional approach to determine the effective parameters characterizing transport phenomena in heterogeneous media is numerical solution of the governing equations with appropriate boundary conditions at the phase interface. An alternative approach for predicting effective physical properties of heterogeneous media is based on statistical continuum theories.[7–12] They concern the effective physical characteristics of heterogeneous media, the local properties of which can be regarded as random functions of position. Thus, the key quantities in statistical continuum theories are probability functions, which correlate the geometrical microstructure of the materials to their effective physical characteristics.

Brown[13] first proposed to use n-point probability functions in order to correlate the geometrical microstructure of a heterogeneous material to its effective physical characteristics. Because the infinite set of correlation functions that characterize the microstructure of a heterogeneous medium[1,13] is never known exactly, an important approach is to devise bounds or approximations on the effective property that utilize lower-order correlation functions to capture salient features of the microstructure. Hashin and Shtrikman[14] derived the best possible two-point bounds (i.e., involving two-point probability functions) on the effective magnetic permeability for isotropic two-phase materials, given just volume-fraction information. For reasons of mathematical analogy, the same bounds can be applied to electrical or heat conductivity and diffusivity. Later, Beran[15] derived bounds for two-phase isotropic composites, which involve sixfold integrals of certain three-point correlation functions and improve the Hashin-Shtrikman bounds. Torquato[16] and Milton[17] independently simplified the three-point Beran bounds and showed that they can be expressed in terms of the volume fractions and the single three-point microstructural parameter ζ_2, which is a multidimensional integral involving the three-point probability function. The same microstructural parameter is involved in expressions approximating the effective conductivity and diffusion coefficient.[11,18,19] Thovert *et al.*[20] derived analytically

a)Authors to whom correspondence should be addressed. Electronic addresses: tallarek@staff.uni-marburg.de and torquato@electron.princeton.edu.

expressions to compute the three-point microstructural parameters exactly through the first order in the volume fraction for equilibrium random packings of polydisperse hard spheres. The authors utilized the expressions to derive rigorous bounds on the effective conductivity and elastic modulus. Recently, Gillman and Matouš[21] and Gillman *et al.*[22] employed the three-point microstructural parameters to predict the effective thermal conductivity and thermomechanical properties of random packs of spheres, ellipsoids, and Platonic solids. The authors proposed new adaptive methods to evaluate accurately the three-point microstructural parameters using a Monte Carlo-based statistical sampling algorithm.[21,22]

In a previous paper[23] we analyzed the impact of packing microstructure on the effective diffusivity in random packings of monosized hard spheres. The effective diffusion coefficient D_{eff} was evaluated by the approximate analytical formula developed by Torquato,[18,19] involving the three-point microstructural parameter ζ_2. In general, the calculation of ζ_2 requires knowledge of the three-point correlation function S_3, which determines the probability of finding three points that define the vertices of a triangle in the interstitial void space of a packing for all side lengths of the triangle. The determination of S_3 in random heterogeneous media is a nontrivial computational task, and in that study we used a numerical approach developed by Miller and Torquato[24] to sample ζ_2 without need to directly pointwise evaluate the three-point probability function. Here, we utilize an alternative approach to compute ζ_2. It comprises the adaptation of a Monte Carlo statistical sampling algorithm of Smith and Torquato[25,26] for the numerical determination of the two- and three-point correlation functions S_2 and S_3. We apply this approach to evaluate the effective diffusion coefficient in random packings of polydisperse spherical particles, which more realistically model suspensions and granular media that arise in industrial and natural situations.

In this work, we generated random bulk packings of polydisperse spheres with solid volume fraction ϕ from 0.54 up to 0.634 based on experimentally measured particle size distributions (PSDs) of microparticles used for the preparation of chromatographic columns. The two before-mentioned values of ϕ reflect the density of, respectively, random loose and maximally random jammed packings of monosized spheres. Our knowledge about the latter value for packings of polydisperse particles is still limited.[1,27,28] It was demonstrated that disordered strictly jammed binary sphere packings can be produced with solid volume fraction well above 0.634.[29] However, the determination of the maximally random jammed state for polydisperse hard-sphere systems is an unresolved problem. Generally, the highest achievable packing density depends on the PSD and packing preparation protocol (algorithmic or experimental). The range of solid volume fractions analyzed in this study ($0.54 \leq \phi \leq 0.634$) reflects the experimental one observed for the bulk bed region in chromatographic columns slurry-packed with microparticles having the same PSDs that we employed here for the computer-generated packings. The three-point parameter ζ_2 was determined for each generated packing, following numerical evaluation of the two-point and three-point probability functions. Calculated values of ζ_2 were used to estimate effective diffusion coefficients via Torquato's approximate formula.[18,19] The D_{eff}-values were then compared with those obtained from the simulation of diffusion in the packings using a random-walk particle-tracking (RWPT) technique. In Sec. II, we provide the details of the numerical approaches used for the generation of the random packings of polydisperse hard spheres, the simulation of diffusion with the RWPT approach, and the calculation of the three-point microstructural parameter ζ_2. Results are presented and discussed in Sec. III.

II. NUMERICAL METHODS

A. Generation of random polydisperse sphere packings

The investigated polydisperse sphere packings are unconfined, bulk packings that mimic infinitely wide packings without walls. The size distributions of the spheres in the generated narrow-PSD and wide-PSD packings were modeled after the experimentally determined PSDs of sub-3 μm core-shell and sub-2 μm fully porous particles, respectively, which by their mean size and size distribution represent modern adsorbents used as packing materials in liquid chromatography. All packings were generated over a range of solid volume fractions between $\phi = 0.54$ and $\phi = 0.634$ to cover the same range as in our previous work with monodisperse packings.[23] A fixed packing protocol was followed with all packing types (monodisperse, narrow-PSD, and wide-PSD packings). This approach eliminates the influence of the experimental packing process in chromatographic practice as well as of all particle properties other than the size distribution and enables the comparison of the monodisperse, narrow-PSD, and wide-PSD packings at equal solid volume fraction.

Bulk, isotropic, random packings of hard, impermeable spheres were generated based on the PSDs of sub-3 μm Kinetex particles (Phenomenex, Torrance, CA) and sub-2 μm Acquity particles (Waters, Milford, MA) as determined by scanning electron microscopy.[30] A JSM-7500F scanning electron microscope (JEOL, Eching, Germany) was used to acquire 44 and 93 images of sets of individual particles, from which 976 and 2608 diameters, respectively, of Kinetex and Acquity particles were manually measured. Afterwards, the experimental data (histograms) were converted into continuous probability density functions (PDFs) using the kernel density estimation method with Gaussian kernel and restriction to positive values.[31] The experimental histograms for the PSDs and the resulting PDFs are shown in Fig. 1. These two types of particles are characterized by different values of their number-mean diameter $d_p = 2.60$ and 1.64 μm and standard deviation $\sigma = 0.088$ and 0.415 μm for Kinetex and Acquity particles, respectively. Hereinafter, the PSDs corresponding to Kinetex and Acquity particles are referred to as narrow and wide PSD, respectively. The statistical properties of the experimentally determined PSDs and the corresponding PDFs are summarized in Table I.

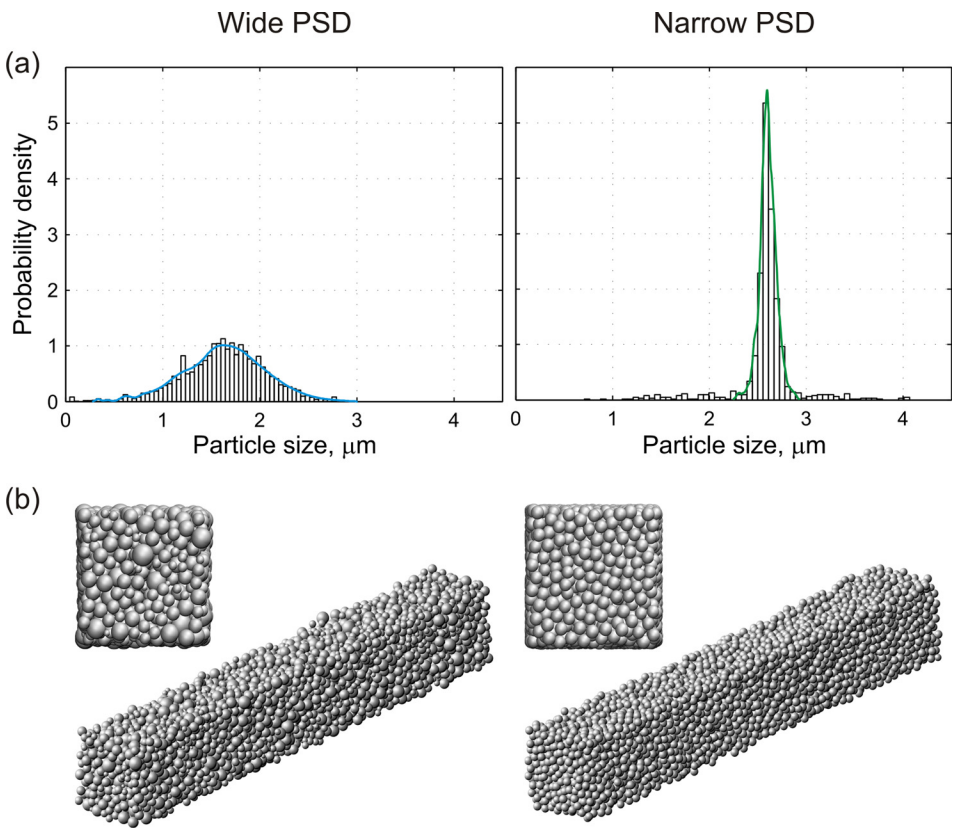

FIG. 1. (a) Wide and narrow particle size distributions (PSDs) as experimentally determined by scanning electron microscopy. Histograms were converted into probability density functions for the computer-generation of polydisperse random hard-sphere packings. (b) Front and side views on a computer-generated wide-PSD packing (left) and narrow-PSD packing (right) at a solid volume fraction $\phi = 0.634$.

Next, arrays of random numbers to represent sphere diameters with the narrow and wide PSDs were generated from the PDFs with a Monte Carlo acceptance-rejection method.[32] Based on the experimental PSDs, two sets of packings at six solid volume fractions ($\phi = 0.54$, 0.56, 0.58, 0.60, 0.634) were generated with periodic boundary conditions in all directions by a Jodrey–Tory (JT) algorithm[33] adopted to the simulation of polydisperse sphere packings.[34,35] Briefly, the modified JT-packing algorithm starts from the generation of a population of spheres with diameters governed by a given PSD. Then, the n centers of the spheres from that population are randomly distributed in a simulation container with volume V, where sphere overlap is typical in the initial configuration. In our case, the container was a rectangular box with dimensions of $10d_p \times 10d_p \times 70d_p$. These packing dimensions were chosen originally for the analysis of hydrodynamic dispersion, where long packings ($\sim 70d_p$) are required to observe asymptotic behavior of the longitudinal dispersion coefficient in fluid flow through a packing at Péclet numbers up to ~ 500.[30,36] Although shorter packings would suffice to observe asymptotic diffusion behavior (without flow), we used the long packings to extend the sample size, i.e., the long packings count as several realizations of shorter packings. The value of n is defined from the targeted (final) solid volume fraction ϕ, the container volume V, and the individual sphere diameters d_i according to

$$\phi = \frac{\pi}{6V} \sum_{i=1}^{n} d_i^3 \tag{1}$$

and varied from 5872 up to 8459, which is sufficiently large to minimize finite-size effects.[36] Then, the iterative packing procedure starts. Each iteration consists of two sequential steps: (i) the search of two sphere centers C_i and C_j with minimum relative pairwise distance $d_{ij,\min}$

$$d_{ij,\min} = \frac{(d_{i,\min} + d_{j,\min})^2}{2(d_i + d_j)}, \tag{2}$$

TABLE I. Statistical properties of the experimentally determined particle size distributions (PSDs) and the corresponding probability density functions (PDFs).

	Narrow PSD (Kinetex)		Wide PSD (Acquity)	
	Experimental data	PDF	Experimental data	PDF
Number of measured particle diameters	976	–	2608	–
Number-mean diameter (d_p), μm	2.60	2.60	1.64	1.64
Standard deviation (σ), μm	0.088	0.088	0.415	0.425
Min. diameter, μm	2.27	2.24	0.30	0.27
Max. diameter, μm	2.90	2.93	2.79	3.01

where $d_{i,\min}$ and $d_{j,\min}$ correspond to the largest sphere diameters at which no overlap occurs between ith and jth spheres; and (ii) asymmetrical spreading apart of these two sphere-center positions along a line C_iC_j up to a new distance ($d_{ij,\max}$) according to the equation

$$d_{ij,\max} = d_{ij,\min} + \Delta_{i,\max} + \Delta_{j,\max}, \tag{3}$$

where $\Delta_{i,\max}$ and $\Delta_{j,\max}$ are determined with Eqs. (4) and (5), respectively,

$$\Delta_{i,\max} = d_{ij,\min}\Omega \log_{10}\frac{d_i}{2d_{i,\min}}, \tag{4}$$

$$\Delta_{j,\max} = d_{ij,\min}\Omega \log_{10}\frac{d_j}{2d_{j,\min}}. \tag{5}$$

The relative spreading of the two sphere centers $\Delta_{i,\max}/\Delta_{j,\max}$ is proportional to the ratio of their final diameters d_i/d_j. As $d_{i,\min}$ and $d_{j,\min}$ asymptotically approach d_i and d_j, the current solid volume fraction approaches ϕ. The scaling factor Ω defines the magnitude of the sphere-center displacements in Eqs. (4) and (5). It also determines the number of iterations required to achieve a targeted solid volume fraction. Though a larger value of Ω increases the convergence rate of the packing algorithm at low targeted solid volume fractions, it can slow down the algorithm at higher values of ϕ. We used $\Omega = 10^{-3}$ to generate all packings analyzed in this study.

The periodic boundary conditions employed for the packing generation allow to approximate infinite systems. Realization of periodic boundaries assumes that the sphere position on one side of a packing (within the rectangular box) influences the position of spheres at the opposite side. As a result, the space is filled regularly while reproducing the representative domain (the rectangular box), but randomness prevails locally within this domain.

B. Simulation of diffusion

Similar to our previous paper,[23] diffusion in the generated packings was simulated using a RWPT technique,[37] where a large number $N = 5 \times 10^6$ of point-like tracers was distributed randomly and uniformly throughout the packing void space. Then, each tracer was iteratively displaced due to random (Brownian) motion calculated from a Gaussian distribution with a mean of zero and a standard deviation of $(2D_m\delta t)^{1/2}$ around each spatial coordinate ($D_m = 1.0 \times 10^{-9}$ m^2 s^{-1}). The value of the time step δt was defined such that the maximum tracer displacement at each iteration did not exceed a distance of $d_p/60$. A multiple-rejection boundary condition was realized at the spheres surface.[38] The position of all tracers was monitored at each time step δt. Diffusion coefficients $D(t)$ in a given direction were calculated from the tracer displacements[39] as

$$D_x(t) = \frac{1}{2N}\frac{d}{dt}\sum_{i=1}^{N}(\Delta r_{xi} - \langle \Delta r_x \rangle)^2, \tag{6}$$

where Δr_{xi} and $\langle \Delta r_x \rangle$ denote the corresponding Cartesian components of the displacement of the ith tracer and the average displacement of the tracer ensemble after time t, respectively, in x-direction. The effective diffusion coefficients D_{eff} were determined from the asymptotes of the $D(t)$-curves.[23] Isotropic diffusion behavior was observed for all sphere packings. The above modeling approach was previously validated[23] by a comparison of the D_{eff}-values simulated in simple cubic and face-centered cubic sphere packings with those determined from the analytical approach after Blees and Leyte.[40] The program realization of the RWPT-algorithm was implemented as parallel code in C language using the Message Passing Interface (MPI) standard.[41] The total simulation time for all sphere packings was ~8 h on 512 BlueGene/P processor cores.

C. Sampling of ζ_2

Based on the approximate formula developed by Torquato for the effective conductivity of particle dispersions,[18] the effective diffusion coefficient in the void space of a packing of hard and impermeable spheres can be evaluated as follows:[19,23]

$$D_{eff} \approx \frac{D_m}{1-\phi}\frac{1-\phi-0.5(1-\phi)\zeta_2}{1+0.5\phi-0.5(1-\phi)\zeta_2}, \tag{7}$$

where ζ_2 is the three-point microstructural parameter defined by[1]

$$\zeta_2 = 1 - \frac{9}{2\phi(1-\phi)}\int_0^\infty \frac{dr}{r}\int_0^\infty \frac{ds}{s}\int_{-1}^{1} d(\cos\theta)P_2(\cos\theta) \times \left[S_3(r,s,\theta) - \frac{S_2(r)S_2(s)}{S_1}\right]. \tag{8}$$

The quantities S_1, $S_2(r)$, and $S_3(r, s, \theta)$ are, respectively, the probabilities of finding in the interparticle void space (i) a single point, (ii) the end points of a line segment of length r, and (iii) the vertices of a triangle with two sides of length r and s and angle θ between them. P_2 is the Legendre polynomial of order two. S_1, S_2, and S_3 are sometimes also referred to as the one-, two-, and three-point probability (or correlation) functions, respectively.[42] Although mathematical formulations of the diffusion and conduction problems are equivalent, there is a relevant distinction between the effective conductivity of a hard sphere packing and the effective diffusion coefficient in the void space of the packing. For the conduction problem, the effective conductivity σ_{eff} characterizes transport properties of the whole medium, i.e., contributions from both phases to the overall transport process are accounted for. By contrast, D_{eff} characterizing transport in the void space of the packing has to be attributed to an effective property of only one phase (the void space). As a consequence, Eq. (7) contains the additional factor $1/(1-\phi)$ as compared to an expression for σ_{eff}.

The one-point probability function S_1 in Eq. (8) is merely the volume fraction of the interparticle void space, $1-\phi$. It can be also evaluated numerically by randomly "tossing" many points and recording the fraction that fall in the interparticle void space. To determine S_2 and S_3, we

adopted an approach proposed by Smith and Torquato,[25,26] which is based on a Monte Carlo statistical sampling. Initially, a large number N_p of primary points was distributed randomly and uniformly throughout the packing space. In this study, we used $N_p = 10^5$. Subsequently, each primary point was designated as the center of a sampling template. A sampling template involves N_φ equally spaced radial rays originating in the primary point and N_ρ concentric circles of radii ρ_k ($k = 0,\ldots, N_\rho - 1$) with centers in the primary point. In Fig. 2(a), a section of the sampling template is shown. Intersections of the radial rays with the circles define the positions of secondary points. Thus, each sampling template consists of the primary point and $N_\rho N_\varphi$ secondary points equiangularly spaced at the discrete distances ρ_k ($k = 0,\ldots, N_\rho - 1$) from the primary point. Further, the orientation of each template was randomized in three-dimensional space by setting random values of the Euler angles (see Fig. 2(b)). The primary point and the secondary points of a given sampling template form a set $\{A\}$ of $N_\rho N_\varphi$ line segments (originating in the primary point) with a range of discrete lengths, ρ_k. The value of $S_2(\rho_k)$ was determined as the probability that the end points of the line segments with length ρ_k reside in the interparticle void space, averaged over $\{A\}$ and the template ensemble. A similar approach was employed to evaluate the values of S_3. For this purpose, a set of triangles (see Fig. 2(a)) formed by all possible combinations of two line segments from $\{A\}$ for each template was constructed. Thus, every triangle was defined by three discrete values corresponding to the lengths of its two sides (ρ_k and ρ_l, with k, $l = 0,\ldots, N_\rho - 1$) and the angle between them (θ_m, with $m = 0,\ldots, N_\varphi - 1$). The value of $S_3(\rho_k, \rho_l, \theta_m)$ was determined as the probability to find the vertices of the triangle defined by ρ_k, ρ_l, and θ_m in the interparticle void space, averaged over $\{A\}$ and the template ensemble. The one-point probability function S_1 was determined as the probability to find the primary and secondary points of the sampling templates in the interparticle void space.

The calculation of ζ_2 by Eq. (8) was carried out by numerical integration using the discrete values of S_2 and S_3, determined as described in the above paragraph. First, Simpson's rule was employed for numerical integration over θ with the substitution $\omega = \cos\theta$, resulting in a function of two variables, $\zeta_2(r, s)$. Then, a two-dimensional trapezoidal rule was used for the r-s integration. Because Eq. (8) includes factors proportional to r^{-1} and s^{-1}, the region of integration near $r = 0$ and $s = 0$ makes a substantial contribution to the integral. This requires using a fine spatial grid to get an accurate value of the integral. On the other hand, Eq. (8) involves the integration over r and s in the range from zero to infinity, and the use of a fine grid results in a very large number of discrete values for S_2 and S_3. In order to meet these conflicting requirements, we employed a nonuniform spatial grid for the construction of the sampling template. With this approach, the radius of the concentric circles increases nonuniformly according to a power law as

$$\rho_k = a_0 d_p A^k, \tag{9}$$

where ρ_k is the radius of the kth circle in the sampling template ($k = 0,\ldots, N_\rho - 1$), a_0 is a constant determining the radius of the smallest circle (ρ_0), and A is a constant larger than unity.

All calculations in this study were performed with sampling templates constructed with $N_\varphi = 64$, $a_0 = 10^{-4}$, $A = 1.21$, and $N_\rho = 64$, resulting in $\rho_0 = 10^{-4} d_p$ (smallest circle radius) and $\rho_{63} \approx 16.42 d_p$ (largest circle radius). Figure 3 shows the normalized circle radius in the sampling template, determined by Eq. (9) with the above set of the parameters a_0, A, and N_ρ as a function of the circle index k. More than 76% of the circles in the template have a radius less than d_p, providing a fine spatial grid resolution for the region of integration near $r = 0$ and $s = 0$. Asymptotic analysis of the calculated two-point and three-point probability functions, presented in Sec. III, shows that the values of

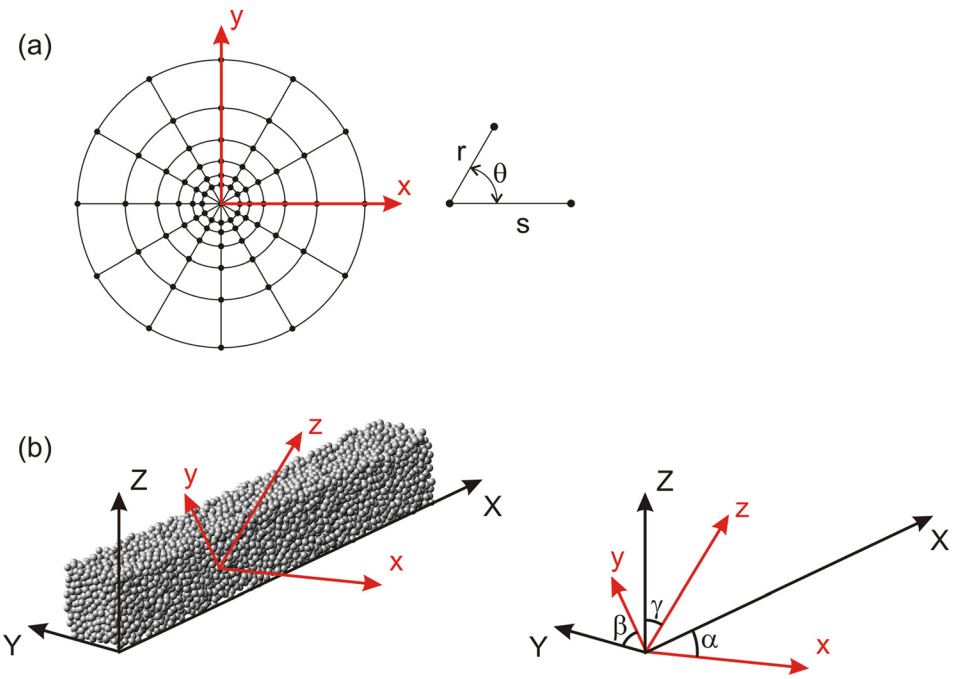

FIG. 2. (a) Section of a sampling template used to evaluate the two-point and three-point probability functions $S_2(r)$ and $S_3(r, s, \theta)$. The primary point is located in the template center. Positions of secondary points are determined by the intersections of the radial rays and concentric circles. The primary point and each secondary point define a line segment characterized by its length r. Two line segments form a triangle characterized by the lengths of its two sides (r and s) and the angle θ. For the present study, 10^5 sampling templates containing 64 circles and 64 equally spaced radial rays were used. (b) The orientation of each template was randomized in three-dimensional space by setting random values of the Euler angles (α, β, and γ) relative to the principal axes of the packing.

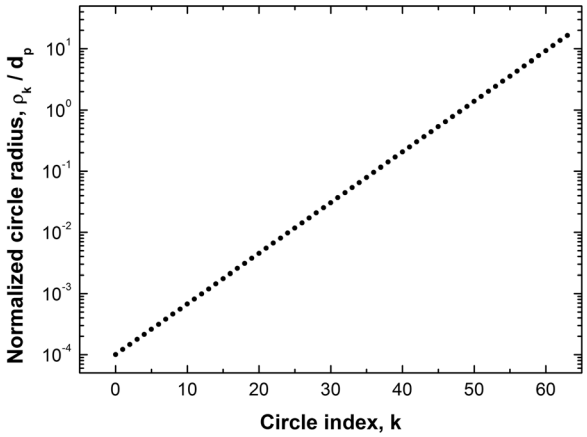

FIG. 3. Normalized radius of the circles (ρ/d_p) in the sampling template, determined by Eq. (9) with $a_0 = 10^{-4}$, $A = 1.21$, and $N_\rho = 64$, as a function of the circle index. The smallest ($k = 0$) and the largest ($k = 63$) circle radius are $10^{-4}d_p$ and $\sim 16.42d_p$, respectively.

$S_2(r)$ and $S_3(r, s, \theta)$, determined for $r = \rho_0$ and $r = s = \rho_{63}$, are very close to the theoretical ones for $r \to 0$ and $r, s \to \infty$, respectively.

III. RESULTS AND DISCUSSION

The accuracy of calculation of the microstructural parameter ζ_2 by Eq. (8) depends on the precision of the numerical integration procedure and determination of the two-point and three-point probability functions. The general properties of the n-point probability functions have been studied by Frisch and Stillinger[43] and Torquato and Stell.[42,44] In particular, S_2 and S_3 in a statistically homogeneous and isotropic two-phase random medium without long-range order exhibit the following asymptotic properties

$$\lim_{r \to 0} S_2(r) = 1 - \phi, \tag{10}$$

$$\lim_{r \to \infty} S_2(r) = (1 - \phi)^2, \tag{11}$$

$$\lim_{\substack{r \to 0 \\ s \to 0}} S_3(r, s, \theta) = 1 - \phi, \tag{12}$$

$$\lim_{\substack{r \to \infty \\ s \to \infty \\ t \to \infty}} S_3(r, s, \theta) = (1 - \phi)^3 \quad \text{with } t = (r^2 + s^2 - 2rs\cos\theta)^{1/2}, \tag{13}$$

where S_2 and S_3 are determined for the phase with volume fraction ϕ.

Figures 4 and 5 show the two-point probability functions $S_2(r)$ for the packings with wide PSD (left panels) and narrow PSD (right panels) at $\phi = 0.54$ and 0.634, determined by the sampling template approach. According to Eq. (10), $S_2(r)$ takes on the value $1 - \phi$, if the distance between the points approaches zero ($r \to 0$). Figure 4 indicates excellent agreement between the calculated two-point probability functions and the theoretical asymptotic values equal to 0.46 and 0.366 at $\phi = 0.54$ and 0.634, respectively, which are shown in the figure as the dashed lines. The same perfect coincidence of calculated and theoretical asymptotic values was observed also at all other solid volume fractions (data not shown): The relative difference between the theoretical values of $S_2(r \to 0)$ and their values calculated at $r/d_p < 10^{-3}$ does not exceed 0.3%. If the distance between two points becomes very large (i.e., $r \to \infty$), $S_2(r)$ approaches $(1 - \phi)^2$ (see Eq. (11)). In Fig. 5, we present the calculated values of $S_2(r)$ along with their theoretical values for $r \to \infty$ equal to 0.2116 and 0.1340 at $\phi = 0.54$ and 0.634, respectively, according to Eq. (11). Already for $r \approx 10d_p$, the numerically determined S_2 is very close to the corresponding theoretical value $S_2(r \to \infty)$ for all four packings presented in the figure. Very good agreements were also observed at all other values of ϕ (data not shown): The relative difference between the theoretical values of $S_2(r \to \infty)$ and their values calculated at $r/d_p > 10$ does not exceed 0.5%. The main conclusion which can be drawn from the data presented in Figs. 4 and 5 is that the use of the finite range ($10^{-4}d_p \le r \le 16.42d_p$) for the distance between two points allows to reproduce very accurately the asymptotic behavior of the two-point probability function $S_2(r)$ at $r \to 0$ and $r \to \infty$ in the packings we analyzed in this study.

A similar asymptotic analysis was carried out for the three-point probability function $S_3(r, s, \theta)$. In Figs. 6(a) and 6(b), we compare the numerically determined $S_3(r = 10^{-4}d_p, s = 10^{-4}d_p, \theta)$ with the theoretical values defined by Eq. (12). According to Eq. (12), if two pairwise distances between three points approach zero, the three-point probability function approaches $(1 - \phi)$. We again observe a very good agreement between the numerical and theoretical values (the relative difference is less than 0.35%). If all pairwise distances between three points approach infinity, then $S_3 = (1 - \phi)^3$ according to Eq. (13). In Figs. 7(a) and 7(b), we compare the

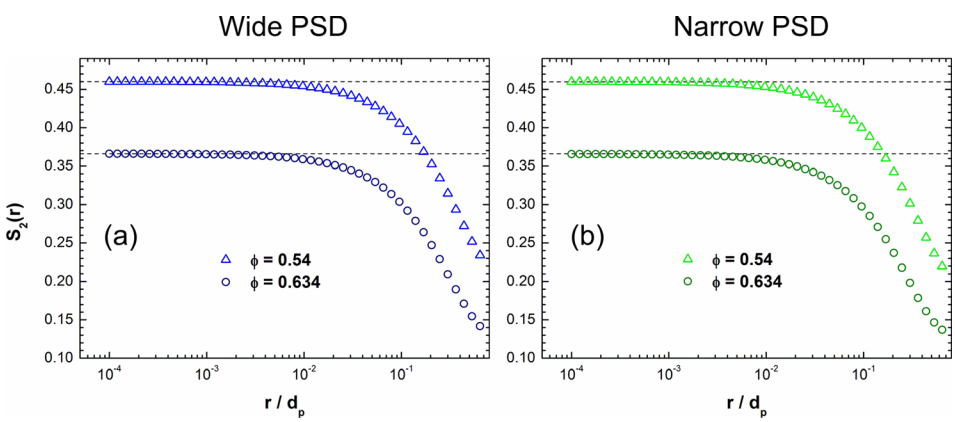

FIG. 4. Two-point probability function $S_2(r)$, calculated using the sampling templates, for polydisperse packings with (a) wide PSD and (b) narrow PSD at two solid volume fractions, $\phi = 0.54$ and 0.634. The smallest value of r in both panels is $10^{-4}d_p$. The dashed lines indicate the corresponding theoretical values for $S_2(r \to 0)$ defined by Eq. (10). The value of r is normalized by the corresponding mean particle diameter d_p (cf. Table I).

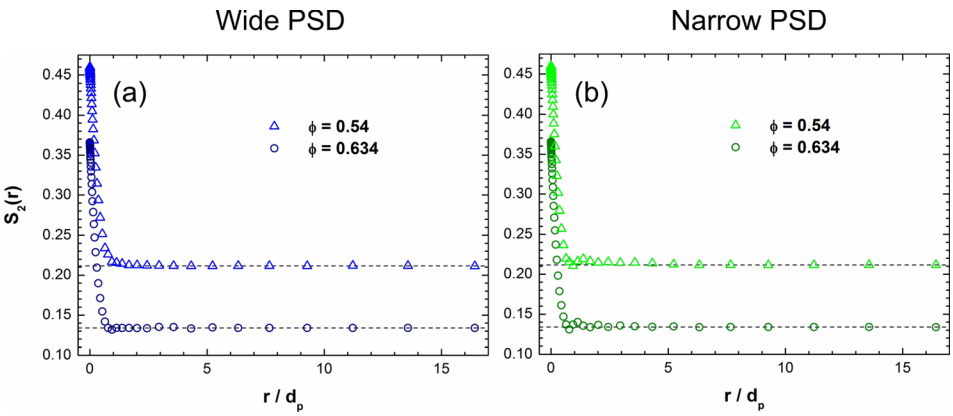

FIG. 5. Two-point probability function $S_2(r)$, calculated using the sampling templates, for polydisperse packings with (a) wide PSD and (b) narrow PSD at two solid volume fractions, $\phi = 0.54$ and 0.634. The dashed lines indicate the corresponding theoretical values for $S_2(r \rightarrow \infty)$ defined by Eq. (11). The value of r is normalized by the corresponding mean particle diameter d_p (cf. Table I).

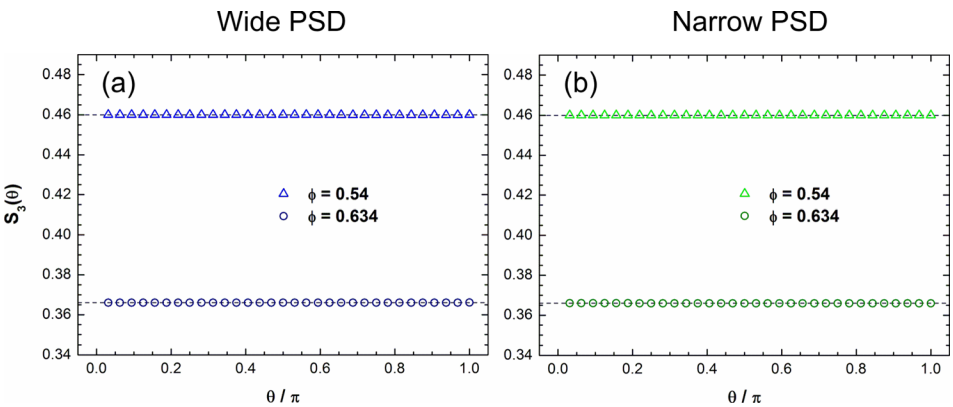

FIG. 6. Three-point probability function $S_3(r = 10^{-4}d_p, s = 10^{-4}d_p, \theta)$ vs. the normalized angle θ/π (cf. Fig. 2(a)), calculated using the sampling templates, for polydisperse packings with (a) wide PSD and (b) narrow PSD at two solid volume fractions, $\phi = 0.54$ and 0.634. The dashed lines indicate the corresponding theoretical values defined by Eq. (12).

values of S_3 determined for $r = 16.42d_p$ and $s = 16.42d_p$ as a function of θ. Independent from θ, the calculated three-point probability functions satisfy very well the theoretical limit given by Eq. (13).

We estimated the overall accuracy of the determination of the two-point and three-point probability functions S_2 and S_3 as well as the numerical integration procedure, which was used to calculate the three-point microstructural parameter ζ_2 with Eq. (8). For this purpose, we compared ζ_2 calculated for regular arrays of hard spheres following the presented approach with theoretical values. McPhedran and Milton[45] computed ζ_2 analytically for cubic lattices of spheres as a function of ϕ. In Figs. 8(a) and 8(b), we compare the ζ_2-values for face-centered cubic (FCC) and body-centered cubic (BCC) sphere arrays calculated by the numerical approach described in Sec. II C (open red circles) with the values obtained analytically by McPhedran and Milton (solid circles). The data in Fig. 8 indicate that the numerical approach we used allows to determine ζ_2 with high accuracy over a wide range of solid volume fractions, including the close packing limit, $\phi \approx 0.68$ and 0.74 for BCC and FCC, respectively.

Subsequently, we employed the proposed numerical approach to calculate ζ_2 in the generated random packings of polydisperse particles. Figure 9 shows ζ_2-values computed by Eq. (8) for narrow-PSD packings (green circles) and wide-PSD packings (blue circles) as a function of ϕ. These values were obtained for 10 different random realizations (i.e., for different random positions of the primary points and random values of the Euler angles) of 10^5 sampling templates for each packing. Thus, the total amount of the primary and secondary points used to determine the probability functions in each packing was greater than 4×10^9. The symbols in Fig. 9 denote the average values of ζ_2 and the error

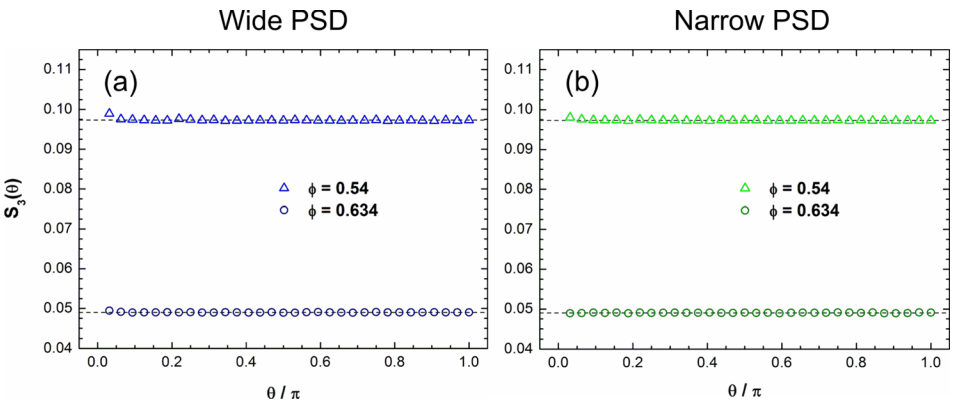

FIG. 7. Three-point probability function $S_3(r = 16.42d_p, s = 16.42d_p, \theta)$ vs. the normalized angle θ/π (cf. Fig. 2(a)), calculated using the sampling templates, for polydisperse packings with (a) wide PSD and (b) narrow PSD at two solid volume fractions, $\phi = 0.54$ and 0.634. The dashed lines indicate the corresponding theoretical values defined by Eq. (13).

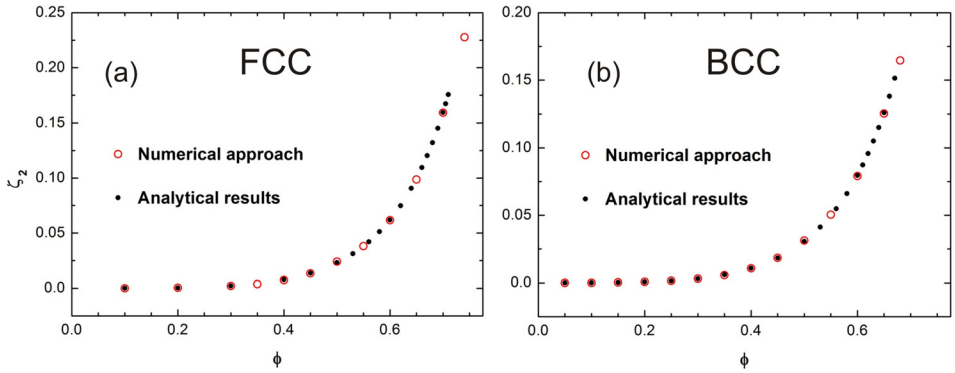

FIG. 8. Comparison of the three-point microstructural parameter ζ_2 obtained by the numerical approach using the sampling templates (open circles) and calculated with the analytical approach[45] (solid circles) for (a) face-centered cubic and (b) body-centered cubic sphere arrays as a function of the solid volume fraction ϕ.

bars indicate 95% confidence intervals calculated using the standard error of the mean. The small error bars (their height does not exceed 0.6% of the corresponding ζ_2-value) allow to conclude that the set of 10^5 sampling templates is statistically representative to evaluate ζ_2 with high accuracy. Additionally, we carried out sampling calculations of ζ_2 (for a wide-PSD packing with $\phi = 0.634$) using a larger number of templates ($N_p = 2 \times 10^5$ and 5×10^5) and higher values of the template parameters $N_\phi = 128$ and $N_\rho = 128$ to analyze the influence on computational accuracy. With these template parameters, the calculated mean values of ζ_2 differed from the corresponding value in Fig. 9 by less than 0.15%. For $N_p = 2 \times 10^5$ and 5×10^5, the confidence interval was, respectively, 81% and 67% relative to that for $N_p = 10^5$, $N_\varphi = 64$, and $N_\rho = 64$. These results indicate that the chosen values of the sampling template parameters allow to determine ζ_2 with high accuracy. The results in Fig. 9 indicate that both packing density and the particles' polydispersity affect ζ_2. The ζ_2-values increase with the solid volume fraction for both types of polydisperse packings. At a given ϕ, the narrow-PSD packings (green circles) have a larger ζ_2-value than the wide-PSD packings (blue circles), but this difference decreases with increasing packing density.

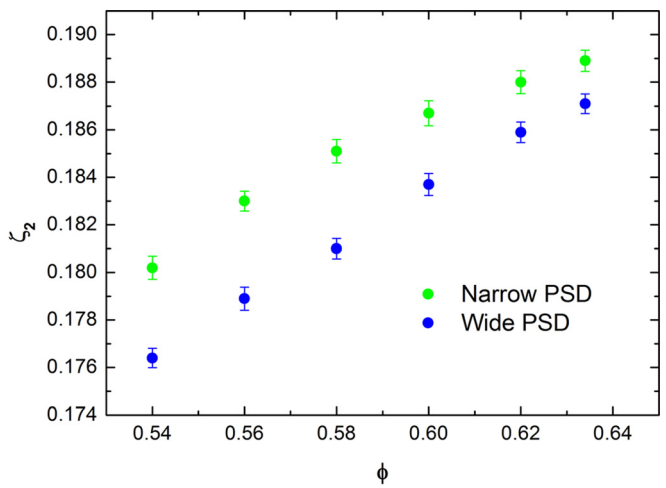

FIG. 9. Three-point microstructural parameter ζ_2 calculated with Eq. (8) as a function of the solid volume fraction ϕ of the polydisperse packings with narrow and wide PSDs (cf. Table I). Each value of ζ_2 corresponds to the average from 10 different realizations of 10^5 sampling templates. The error bars indicate 95% confidence intervals calculated using the standard error of the mean.

The obtained values of the three-point microstructural parameter were used to calculate the effective diffusion coefficient by Eq. (7). Figure 10 shows the normalized D_{eff} (open circles) as a function of the solid volume fraction, determined for monodisperse, the wide-PSD, and the narrow-PSD packings. The effective diffusion coefficients in all three packing types demonstrate the same trend and decrease with increasing solid volume fraction. This can be easily understood from the decrease of the interstitial void space between particles, which obstructs diffusive transport. In contrast to the results for ζ_2, the effective diffusion coefficient is hardly sensitive to the PSDs. At a given ϕ, the relative difference between D_{eff}-values in the analyzed packing types does not exceed 0.5%. The monodisperse packings are always characterized by the smallest D_{eff}/D_m-values, whereas the wide-PSD packings have the largest values. Compared with the results from our RWPT simulations, the presented approach slightly overestimates the effective diffusion coefficients. However, the relative difference between D_{eff}-values obtained by the two approaches does not exceed 4% at a given ϕ and PSD. Thus, the proposed approach allows to get a good estimate for the effective diffusion coefficient in polydisperse packings, using only information on packing geometry. In future work, it will be interesting to carry out analogous diffusion studies for disordered jammed

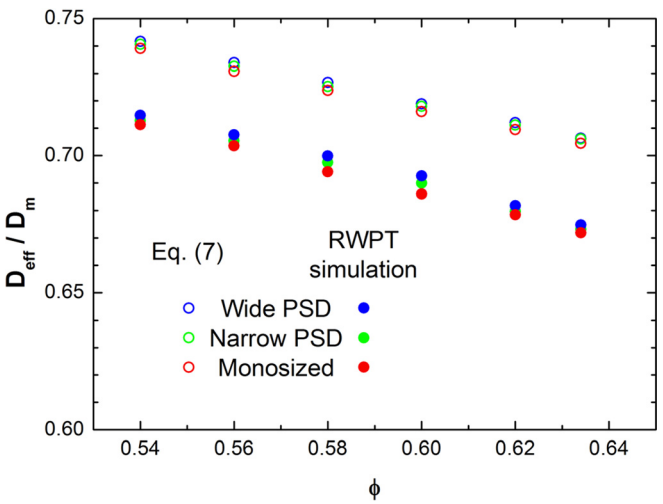

FIG. 10. Normalized effective diffusion coefficients D_{eff}/D_m in monodisperse, narrow-PSD, and wide-PSD random hard-sphere packings as a function of the solid volume fraction ϕ, calculated by Eq. (7) (open circles) and obtained from the RWPT simulations (solid circles).

polydisperse packings produced by the recent Torquato-Jiao algorithm, which can yield anomalously high packing densities.[29] But the presented approach to determine S_2 and S_3 (and estimate D_{eff}) goes beyond computer-generated packings. It can be applied to analyze structure-transport relationships in real material structures obtained from a three-dimensional reconstruction of particulate, monolithic, or consolidated porous media based on, e.g., advanced electron microscopy,[46–51] X-ray tomography,[52–55] or confocal laser scanning microscopy.[56–60]

IV. CONCLUSIONS

This work reports on results obtained for the effective diffusion coefficient D_{eff} in random packings of polydisperse hard spheres. Packings with solid volume fraction from 0.54 up to 0.634 were computer-generated at a fixed generation protocol based on experimentally measured PSDs of microparticles used for the preparation of chromatographic columns. The combination of a computer-generation protocol with real PSDs allowed us to study industrially relevant packings without influence of the experimental packing procedure as well as of all particle properties other than the PSD. In general, this enables the comparison of monodisperse, narrow-PSD, and wide-PSD packings at equal solid volume fraction and was used here to generate the sets of packings with systematically varied packing density suitable for the validation of the numerical approach presented in Sec. II C.

The calculation of D_{eff} was carried out using Torquato's approximate formula (Eq. (7)). It involves the three-point microstructural parameter ζ_2, which depends on the two-point and three-point probability functions S_2 and S_3. Our results demonstrate that the value of the effective diffusion coefficient in the investigated packings is determined by their solid volume fraction ϕ, the spatial positions of the spheres, and to a lesser degree by the particles' polydispersity. At a given ϕ, the relative difference between D_{eff}-values in monodisperse, narrow-PSD, and wide-PSD packings does not exceed 0.5%. The effective diffusion coefficients computed by Torquato's approximate formula were compared with D_{eff}-values derived from RWPT simulations in the packings. The relative difference between D_{eff}-values obtained by these fundamentally different approaches does not exceed a few percents. However, the use of the approximate formula allows to determine the effective diffusion coefficient directly from information on the geometrical structure of a packing. This information can be also obtained from three-dimensional physical reconstruction of real heterogeneous materials. Moreover, the proposed approach is extendable to any two-phase composite material, depending neither on the physical properties of the phases, nor on the geometry of the interface between the phases. Thus, the presented approach provides a straightforward route to evaluate the effective transport characteristics of heterogeneous media and to analyze structure-transport relationships in general. We note in passing that the three-point parameter ζ_2 also arises in accurate estimates for the effective conductivity and effective bulk modulus for two-phase composites,[61,62] and hence our results here can immediately yield these effective property estimates for the disordered polydisperse sphere packings studied in the present paper.

ACKNOWLEDGMENTS

This work was supported by the Deutsche Forschungsgemeinschaft DFG (Bonn, Germany) under Grant No. TA 268/9–1. We thank the John von Neumann Institute for Computing (NIC) and the Jülich Supercomputing Center (JSC), Forschungszentrum Jülich (FZJ, Jülich, Germany), for the allocation of a special CPU-time grant (NIC project number: 8214, JSC project ID: HMR10). S.T. was supported by the National Science Foundation under Grant Nos. DMR-0820341 and DMS-1211087.

[1]S. Torquato, *Random Heterogeneous Materials: Microstructure and Macroscopic Properties* (Springer, New York, 2002).
[2]M. Sahimi, *Heterogeneous Materials: Vol. I. Linear Transport and Optical Properties* (Springer, New York, 2003).
[3]T. I. Zohdi and P. Wriggers, *Introduction to Computational Micromechanics* (Springer, New York, 2005).
[4]M. Kachanov and I. Sevostianov, *Effective Properties of Heterogeneous Materials* (Springer, New York, 2013).
[5]H. M. Jaeger, S. R. Nagel, and R. P. Behringer, Rev. Mod. Phys. **68**, 1259 (1996).
[6]T. I. Zohdi, Arch. Comput. Meth. Eng. **20**, 309 (2013).
[7]M. J. Beran, *Statistical Continuum Theories* (Interscience, New York, 1968).
[8]E. Kröner, *Statistical Continuum Mechanics* (Springer, Vienna, 1972).
[9]P. B. Corson, J. Appl. Phys. **45**, 3159 (1974).
[10]N. Phan-Thien and G. W. Milton, Proc. R. Soc. London A **380**, 333 (1982).
[11]A. K. Sen and S. Torquato, Phys. Rev. B **39**, 4504 (1989).
[12]D. T. Fullwood, B. L. Adams, and S. R. Kalidindi, Phys. Solids **56**, 2287 (2008).
[13]W. F. Brown, Jr., J. Chem. Phys. **23**, 1514 (1955); Trans. Soc. Rheol. **9**, 357 (1965).
[14]Z. Hashin and S. Shtrikman, J. Appl. Phys. **33**, 3125 (1962).
[15]M. Beran, Nuova Cimento **38**, 771 (1965).
[16]S. Torquato, Ph.D. thesis, State University of New York at Stony Brook, 1980.
[17]G. W. Milton, Phys. Rev. Lett. **46**, 542 (1981).
[18]S. Torquato, J. Appl. Phys. **58**, 3790 (1985).
[19]Y. Jiao and S. Torquato, Phys. Biol. **9**, 036009 (2012).
[20]J. F. Thovert, I. C. Kim, S. Torquato, and A. Acrivos, J. Appl. Phys. **67**, 6088 (1990).
[21]A. Gillman and K. Matouš, Phys. Lett. A **378**, 3070 (2014).
[22]A. Gillman, G. Amadio, K. Matouš, and T. L. Jackson, Proc. R. Soc. A **471**, 20150060 (2015).
[23]H. Liasneuski, D. Hlushkou, S. Khirevich, A. Höltzel, U. Tallarek, and S. Torquato, J. Appl. Phys. **116**, 034904 (2014).
[24]C. A. Miller and S. Torquato, J. Appl. Phys. **68**, 5486 (1990).
[25]P. Smith and S. Torquato, J. Comput. Phys. **76**, 176 (1988).
[26]P. A. Smith and S. Torquato, J. Appl. Phys. **65**, 893 (1989).
[27]S. Torquato and F. H. Stillinger, Rev. Mod. Phys. **82**, 2633 (2010).
[28]V. Baranau and U. Tallarek, Soft Matter **10**, 3826 (2014); **10**, 7838 (2014).
[29]A. B. Hopkins, F. H. Stillinger, and S. Torquato, Phys. Rev. E **88**, 022205 (2013).
[30]A. Daneyko, A. Höltzel, S. Khirevich, and U. Tallarek, Anal. Chem. **83**, 3903 (2011).
[31]A. W. Bowman and A. Azzalini, *Applied Smoothing Techniques for Data Analysis: The Kernel Approach with S-Plus Illustrations* (Oxford University Press, New York, 1997).
[32]J. E. Gentle, *Random Number Generation and Monte Carlo Methods*, 2nd ed. (Springer, New York, 2003).
[33]W. S. Jodrey and E. M. Tory, Phys. Rev. A **32**, 2347 (1985).
[34]D. Hlushkou, A. Seidel-Morgenstern, and U. Tallarek, Langmuir **21**, 6097 (2005).
[35]D. Hlushkou, F. Gritti, A. Daneyko, G. Guiochon, and U. Tallarek, J. Phys. Chem. C **117**, 22974 (2013).

[36]S. Khirevich, A. Höltzel, and U. Tallarek, Commun. Comput. Phys. **13**, 801 (2013).
[37]F. Delay, P. Ackerer, and C. Danquigny, Vadose Zone J. **4**, 360 (2005).
[38]P. Szymczak and A. J. C. Ladd, Phys. Rev. E **68**, 036704 (2003).
[39]H. Brenner, Philos. Trans. R. Soc. London A **297**, 81 (1980).
[40]M. H. Blees and J. C. Leyte, J. Colloid Interface Sci. **166**, 118 (1994).
[41]W. Gropp, E. Lusk, and A. Skjellum, *Using MPI: Portable Parallel Programming with the Message-Passing Interface*, 2nd ed. (MIT Press, Cambridge, MA, 1999).
[42]S. Torquato and G. Stell, J. Chem. Phys. **77**, 2071 (1982).
[43]H. L. Frisch and F. H. Stillinger, J. Chem. Phys. **38**, 2200 (1963).
[44]S. Torquato and G. Stell, J. Chem. Phys. **82**, 980 (1985).
[45]R. C. McPhedran and G. W. Milton, Appl. Phys. A **26**, 207 (1981).
[46]G. Möbus and B. J. Inkson, Mater. Today **10**, 18 (2007).
[47]H. Koku, R. S. Maier, K. J. Czymmek, M. R. Schure, and A. M. Lenhoff, J. Chromatogr. A **1218**, 3466 (2011).
[48]Z. Saghi and P. A. Midgley, Annu. Rev. Mater. Res. **42**, 59 (2012).
[49]G. Van Tendeloo, S. Bals, S. Van Aert, J. Verbeeck, and D. Van Dyck, Adv. Mater. **24**, 5655 (2012).
[50]T. Müllner, A. Zankel, F. Svec, and U. Tallarek, Mater. Today **17**, 404 (2014).
[51]D. Stoeckel, C. Kübel, K. Hormann, A. Höltzel, B. M. Smarsly, and U. Tallarek, Langmuir **30**, 9022 (2014).
[52]T. Aste, M. Saadatfar, and T. J. Senden, Phys. Rev. E **71**, 061302 (2005).
[53]H. Dong and M. J. Blunt, Phys. Rev. E **80**, 036307 (2009).
[54]C. J. Gommes, A.-J. Bons, S. Blacher, J. H. Dunsmuir, and A. H. Tsou, AIChE J. **55**, 2000 (2009).
[55]F. Chevillotte, C. Perrot, and E. Guillon, J. Acoust. Soc. Am. **134**, 4681 (2013).
[56]J. T. Fredrich, B. Menendez, and T. F. Wong, Science **268**, 276 (1995).
[57]S. Bruns, T. Müllner, M. Kollmann, J. Schachtner, A. Höltzel, and U. Tallarek, Anal. Chem. **82**, 6569 (2010).
[58]S. Bruns and U. Tallarek, J. Chromatogr. A **1218**, 1849 (2011).
[59]S. Bruns, J. P. Grinias, L. E. Blue, J. W. Jorgenson, and U. Tallarek, Anal. Chem. **84**, 4496 (2012).
[60]K. Hormann and U. Tallarek, J. Chromatogr. A **1312**, 26 (2013).
[61]S. Torquato and F. Lado, Phys. Rev. B **33**, 6428 (1986).
[62]S. Torquato, J. Mech. Phys. Solids **45**, 1421 (1997).